JOURNAL OF GEOPHYSICAL RESEARCH, VOL. 113, C04034, doi:10.1029/2006JC003820, 2008

Seasonal temperature dynamics of the upper ocean in the Southern California Bight

Craig G. Gelpi[1] and Karen E. Norris[2]

Received 26 July 2006; revised 10 October 2007; accepted 7 January 2008; published 26 April 2008.

[1] Long-duration temperature measurements from a variety of sources, including island thermographs, CalCOFI cruise archives, NOAA buoys, and coastal piers are analyzed to determine the seasonal dynamics of the upper ocean (0–30 m) in the Southern California Bight. Dynamics in the Bight differ significantly from those found either to the north or south, with seasonal temperatures in the Bight having greater amplitude and peaking earlier in the year. The time of the seasonal peak varies with depth within the inner Bight such that the maximum temperature at 30 m occurs six weeks after the 5-m maximum. In contrast, the water column outside the Bight changes temperature uniformly with depth. A simple diffusion equation is employed to model this change in the inner Bight and estimate the vertical eddy-diffusion coefficient, determined to be 10^{-4} m^2s^{-1}. The CalCOFI data also indicate the seasonal dynamics vary with the phase of the Pacific Decadal Oscillation; during the cold phase there is a smaller seasonal amplitude and later time for maximum temperature.

Citation: Gelpi, C. G., and K. E. Norris (2008), Seasonal temperature dynamics of the upper ocean in the Southern California Bight, *J. Geophys. Res., 113* , C04034, doi:10.1029/2006JC003820.

1. Introduction

[2] The Southern California Bight (SCB) is an indentation of the generally northwest/southeast trending California coastline at Pt. Conception extending south to Baja California, Mexico. It coincides with several unique biological and physical characteristics. Biologically, the Bight forms the transition zone from northern marine populations to more temperate species resulting in 87% of California marine fish species being found there [*Cross and Allen*, 1993]. Physically, wind conditions differ there relative to the rest of the California coast, with wind speeds being lower and wind directions more consistent within the Bight [*Winant and Dorman*, 1997]. Also, water-temperature dynamics in the SCB, especially within the inner Bight, differ pronouncedly from those found off the rest of the California and Mexican coasts. For example, the central Bight does not have the upwelling characteristics of Northern California [*Hickey*, 1992]. As we show below, it warms earlier than either the Central Coast north of it or the offshore region southwest of it.

[3] The Bight has a complex topography, populated by islands, ridges, and basins. This is in distinction to the region north of the Bight, where there is a small continental shelf, and to the south, where the short shelf resumes (see Figure 1). The submarine region has been called the continental borderlands to distinguish it from the simpler shelf topography. We divide the Bight into several regions: the northern Bight, north of the Northern Channel islands; the central Bight, surrounding the Southern Channel islands; and the southern Bight, south of the central Bight toward San Diego, California. We also distinguish the inner central Bight as adjacent to the Los Angeles metropolitan area and including Santa Catalina Island and Santa Monica Bay.

[4] Long-term (10 years) temperature measurements are now available for the near-surface 5 to 30-m water in the center of the Bight. These measurements, discussed in detail in section 3, indicate that the day of maximum temperature changes with depth. This prompted a study of seasonal temperature variation with depth in the upper ocean throughout the Bight. The present study is undertaken to understand the temperature configuration and seasonal dynamics of the upper ocean within the central Bight with the ultimate goal of relating its physical oceanography to the marine biology of the inner Bight, especially Santa Catalina Island.

[5] The next section is a review of the circulation and wind conditions of the Bight as presently understood and includes relevant temperature studies. A description and analysis of the various data sets used in our study follow in section 3. Section 4 describes a simple model for the thermodynamics of the inner Bight and a comparison of its results to the data. All the significant results are summarized, and their implications discussed, in section 5.

2. Review of Circulation and Temperature Studies

[6] The major currents affecting the Bight compose the California Current System (CCS). The main current is the

[1]Catalina Conservancy Divers, Catalina Island Conservancy, Avalon, California, USA.
[2]Department of Atmospheric and Oceanic Sciences, University of California, Los Angeles, California, USA.

0148-0227/08/2006JC003820$09.00

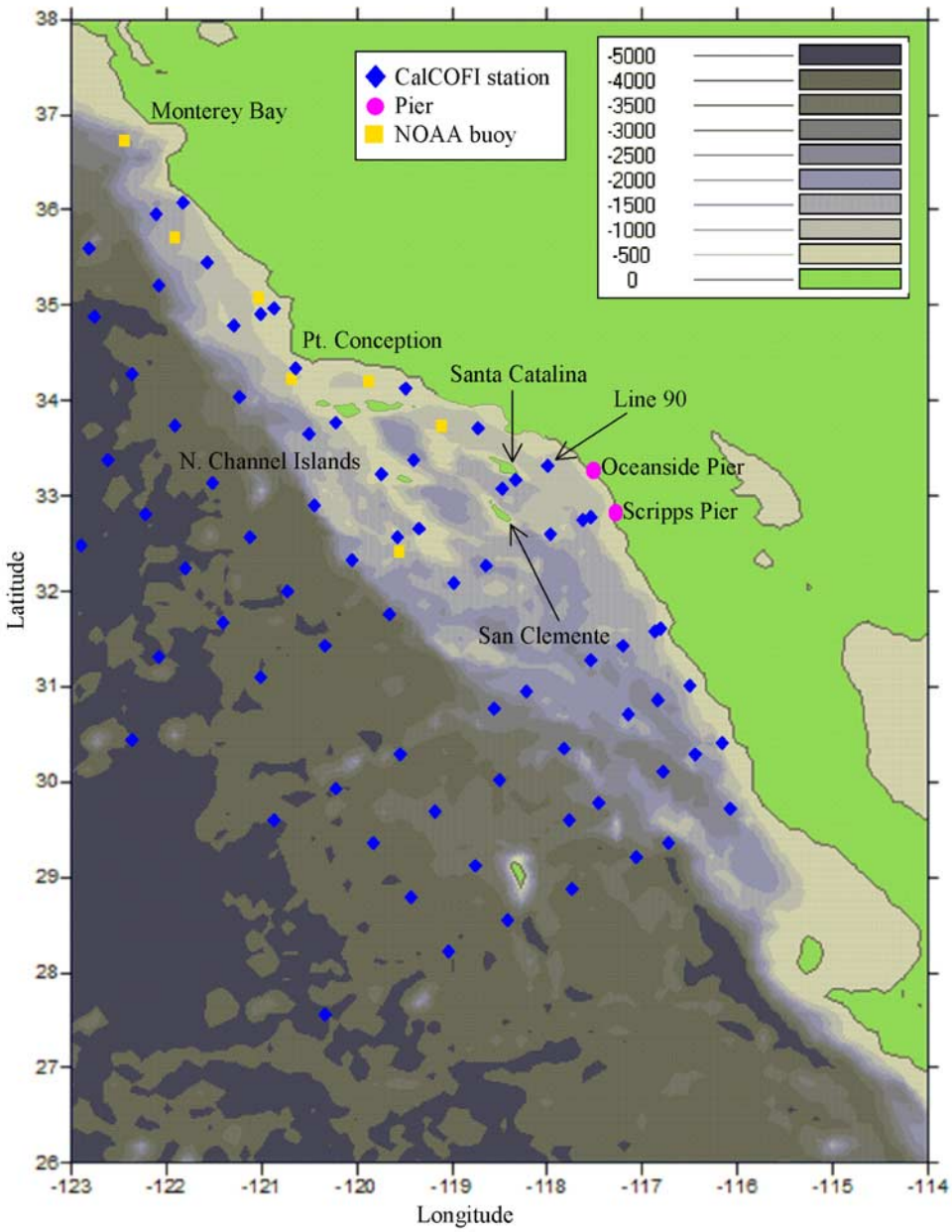

Figure 1. Map of the CalCOFI stations, buoys, and pier sites.

Table 1. Data Sets and Characteristics

Data Set	Spatial Coverage	Temporal Frequency	Temporal Duration	Depth Samples
CalCOFI	broad	quarterly	decades	0, 10, 20, 30, 50 m
NOAA Buoy	broad, seven sites	continuous	1 decade	surface
Catalina Conservancy Divers	limited to S. Catalina Is., four sites	continuous	1 decade	5, 10, 20, 30 m
Channel Islands NP	limited to N. Channel Is., 16 sites	continuous	1 decade	one depth/site
Scripps Pier	one location	continuous	decades	surface
List and Koh	one location	continuous	0.5 decade	surface

California Current, an eastern boundary current that brings water from northern latitudes that is relatively fresh, cold, and nutrient poor. There are two countercurrents in the CCS, the California Undercurrent (CU) and the inshore countercurrent. The CU originates farther south as identified by its higher temperature, salinity, and nutrients [*Lynn and Simpson*, 1987].

[7] The magnitudes and directions of the currents are determined from dynamic height measurements [*Reid*, 1988; *Lynn and Simpson*, 1987, 1990; *Bray et al.*, 1999] and from current meters [*Hickey*, 1992, 1993; *Hamilton et al.*, 2006]. While the undercurrent in the inner Bight is perennially poleward, the surface current is variable, forming the Southern California Eddy that coincides with the offshore equatorward flowing California Current and the inshore poleward flowing counter current. The eddy is weakest in the spring and strongest in the fall and winter.

[8] The transverse mountains of Southern California shelter the inner Bight from the steady strong winds characteristic of the central and northern California coast. *Hickey* [1992], *Winant and Dorman* [1997], *Lynn et al.* [2003], and *Chelton* [1982] have described the impact of the seasonal winds on the CCS. In the winter, winds along the central coast and the outer Bight are similar in magnitude and are generally out of the west and produce no upwelling along the coast. When the northern and central California winds shift to a southeastward direction in the spring there is offshore Ekman transport and accompanying coastal upwelling north of Point Conception. However, in the sheltered inner Bight, the winds remain toward the northeast. By summertime, the regional differences in the wind speed and direction result in a nonzero wind-stress curl within the Bight that produces Ekman pumping with the largest upwelling being 200 km offshore.

[9] Although there have been many studies of temperature variability in the Bight [e.g., *Bratkovich*, 1985; *Lerczak et al.*, 2003; *Pidgeon and Winant*, 2005; *Hamilton et al.*, 2006] there is relatively little work on the seasonal fluctuations, especially using multiyear measurements. Detailed seasonal characteristics are difficult to retrieve from small temporal-length studies as nonstationary features described by *Mendelssohn et al.* [2004] and *Hickey et al.* [2003], as well as episodic events such as El Nino may unduly weight the results.

[10] Work based on longer length measurements [e.g., *List and Koh*, 1976; *Lynn*, 1966; *Winant and Bratkovich*, 1981; *Reid*, 1988; *Nezlin et al.*, 2004] found a well-defined seasonal cycle in the SCB but not off central California.

3. Data Sets

[11] We considered four qualities in choosing temperature data sets to study the SCB's upper-ocean seasonal dynamics:

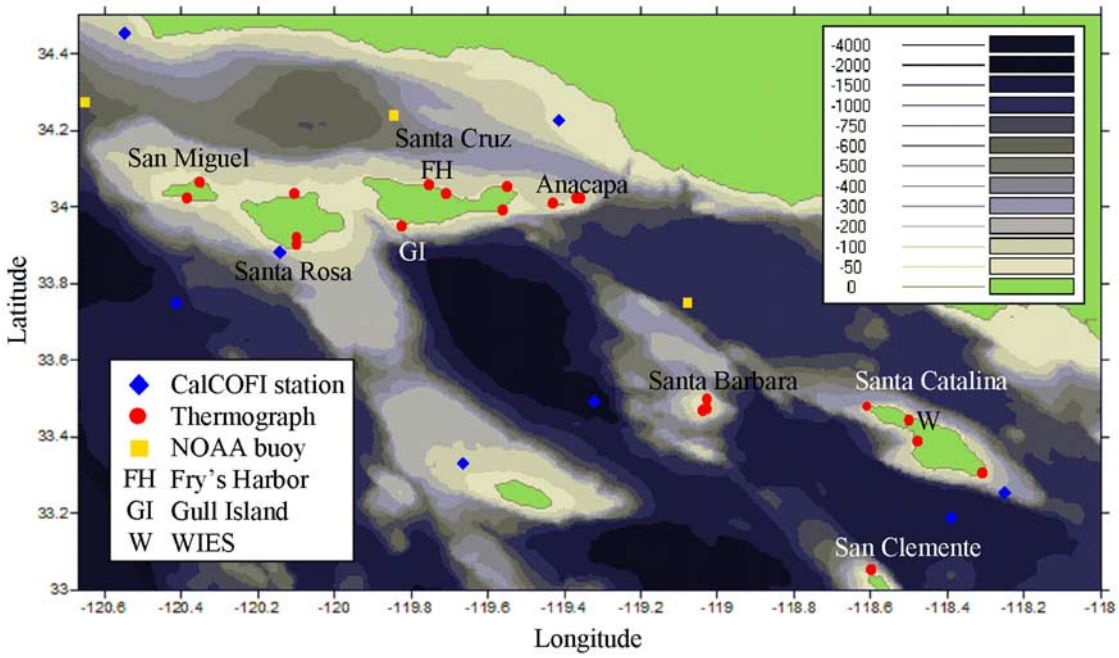

Figure 2. Expanded map indicating the thermograph sites.

Table 2. NOAA Buoy Data Sets

Site	ID	Lat. N	Long. W	Years, Total Years
Tanner Banks	46047	32.43°	119.53°	1991–1993, 1999–2003 (8)
St. Monica Basin	46025	33.75°	119.08°	1991–2003 (13)
St. Barbara East	46053	34.24°	119.85°	1994–1996, 1998–2003 (9)
St. Barbara West	46063	34.27°	120.66°	1998–2003 (6)
Pt. San Luis	46062	35.10°	121.01°	1997–2003 (7)
Cape San Martin	46028	35.74°	121.89°	1993–2003 (11)
Monterey	46042	37.75°	122.42°	1993–2003 (11)

sampling frequency, temporal duration, horizontal spatial extent, and depth coverage. The sampling frequency should be greater than the seasonal Nyquist frequency, i.e., eight samples per year. To properly weight the influence of episodic events, such as El Nino, we like the temporal duration to be on the order of 10 years or greater. The horizontal spatial extent should be broad, i.e., encompassing and extending beyond the Bight so as to distinguish Bight characteristics from those of the CCS. The depth coverage should be capable of distinguishing between upwelling and diffusion effects in the upper ocean, e.g., 10-m depth sampling.

[12] We employed a variety of data sets to meet as many of these criteria as possible. These data sets, together with a brief description of their characteristics, are listed in Table 1, and their spatial distribution is shown in Figures 1 and 2. The common characteristic among the sets is duration, approximately a decade or longer.

[13] Our core data are temperature measurements made by the Catalina Conservancy Divers (CCD). The CCD have maintained thermographs with an accuracy of 0.3°C and hourly sampling around Santa Catalina Island (33° 27′N, 118° 29′W) since 1992. *Gelpi and Norris* [2005] have reported locations of the thermographs and the data processing. For the present work, we used data measured at up to four depths for each of four sites around the island (Figure 2). The thermograph depths are 4.6 m, 9.1 m, 18.3 m, and 30.5 m, with each instrument mounted approximately one-half meter from the bottom. All sites were open to the ocean and experienced the sweep of the along-shore currents. These data provide a long-term, dense temporal series of temperature measurements made in the center of the SCB. Data from the four sites were averaged to yield a single island-wide measurement at each depth. These results are used to measure the seasonal characteristics in the center of the Bight.

[14] The California Cooperative Oceanic and Fisheries Investigation (CalCOFI) provides one of the best known data sets. Data are obtained from cruises nominally executed quarterly. From files of CalCOFI data collections from 1949 to the second quarter of 2003 we retrieved interpolated temperatures and salinity measured at all stations on the CalCOFI lines 70 to 110 (Figure 1) as well as the date of measurement. The standard depths are 0, 10, 20, 30, and 50 m. CalCOFI data give us a long-term time series, sampled in depth and broadly sampled in the horizontal, but relatively sparsely sampled in time. These data are used to ascertain the horizontal extent of the seasonal variations.

[15] The National Oceanic and Atmospheric Administration (NOAA) maintains a line of deep-water buoys along the California coast. The buoys report meteorological data hourly, including water temperature and wind velocity [*Earle*, 1996]. We employed archived data from seven of these buoys, four located in the SCB and three along the Central Coast. With an average collection of 9 years these data sets form a sufficiently long period for this study. The positions of all the buoys and their data collection intervals are listed in Table 2 and their locations are also plotted on the map in Figure 1. These data supplement the broad coverage of CalCOFI with a dense temporal sampling. They also provide an independent measurement of seasonal characteristics within the Bight and included ancillary data such as wind velocity.

[16] Using protocols similar to those of the CCD, the National Park Service at Channel Islands National Park (ChINP) has collected temperature measurements at 16 kelp-forest monitoring sites mostly along the Northern

Table 3. Channel Islands National Park Data Sites

Site	ID	Island	Lat. N	Long. W	Start	Stop	Depth, m
Admiral's Reef	AR	Anacapa	34.01°	119.34°	8/26/1993	8/9/2004	16
Cathedral Cove	CC	Anacapa	34.02°	119.37°	10/1/1993	8/10/2004	6
Landing Cove	LC	Anacapa	34.02°	119.36°	10/1/1993	7/16/2004	5
Boy Scout Camp	BSC	S. Clemente	33.00°	118.55°	5/30/2003	6/22/2004	11
Eel Pt.	EP	S. Clemente	32.92°	118.55°	5/29/2003	6/23/2004	10
Horse Bch Cove	HBC	S. Clemente	32.81°	118.41°	6/21/2003	6/26/2004	13
Northwest Harbor	NWH	S. Clemente	33.04°′	118.60°	5/28/2003	6/24/2004	11
Arch Pt.	AP	S. Barbara	33.49°	119.03°	3/17/1994	6/8/2004	8
Cat Canyon	CAT	S. Barbara	33.46°	119.04°	6/24/1993	6/27/2004	8
SE Sea Lion Rook.	SESL	S. Barbara	33.47°	119.03°	6/22/1993	9/13/2004	15
Fry's Harbor,	FH	Santa Cruz	34.06°	119.76°	8/12/1993	7/15/2004	13
Gull Island	GI	Santa Cruz	33.95°	119.83°	7/26/1993	8/23/2004	15
Pelican Bay	PB	Santa Cruz	34.03°	119.70°	7/16/1993	7/14/2004	8
Scorpion Anch.	SA	Santa Cruz	34.05°	119.55°	1/20.1994	8/12/2004	5
Yellow Banks	YB	Santa Cruz	33.99°	119.56°	8/10/1993	7/12/2004	15
Hare Rock	HR	San Miguel	34.06°	120.36°	5/21/1993	7/27/2004	5
Wyckoff Ledge	WL	San Miguel	34.02°	120.39°	9/14/1993	7/28/2004	13
Johnson's Lee N.	JLNO	Santa Rosa	33.90°	120.10°	7/29/1993	7/29/2004	11
Johnson's Lee S.	JLSO	Santa Rosa	33.90°	120.10°	7/29/1993	7/29/2004	16
Rodes Reef	RR	Santa Rosa	34.03°	120.11 °	9/14/1993	7/27/2004	13

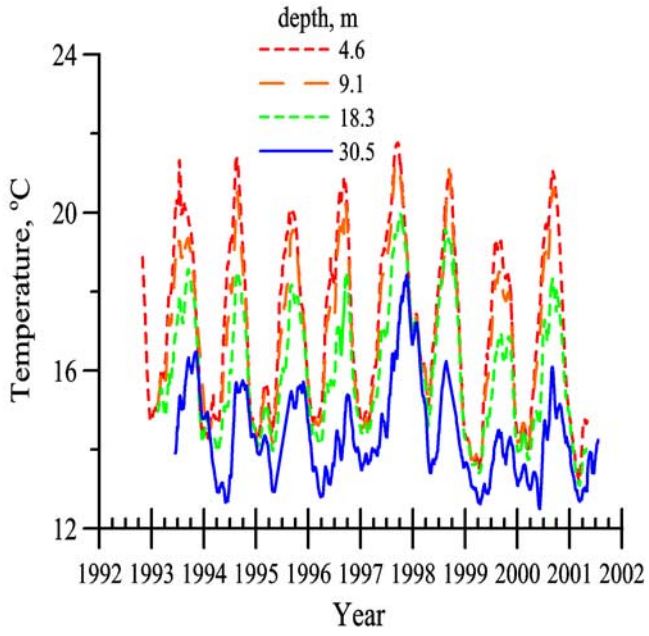

Figure 3. Smoothed CCD data for four depths.

Channel Islands, located about 100 km northwest of Santa Catalina Island [*Davis et al.*, 1997]. The locations, depths and dates of acquisition for the data used in this study are listed in Table 3 and the sites are shown in Figure 2. Temperature was sampled every 5 h for the earlier years and then every hour for the later years. These data provide a dense temporal sampling for the northern SCB similar to those of the CCD instruments, with the exception that the ChINP data are for one depth per site.

[17] Finally, we use surface temperature data collected from two piers in Southern California: Scripps Pier (32°52.02′N, 117° 15.06′W) and Oceanside, 40 km to the north. We use the Scripps data to examine the effects of 1976/1977 regime shift [*Bograd and Lynn*, 2003] on the seasonal parameters. The regime shift is the local expression of the Pacific Decadal Oscillation (PDO) [*Mantua and Hare*, 2002]. These data are the only densely-sampled set that includes significant data collection before and after the regime change. In addition we have digitized plots originally published by *List and Koh* [1976] of the Oceanside pier data. These data were measured near Scripps, but away from the submarine canyon complex that straddles Scripps, and provide an independent measurement of southern Bight conditions. Both pier locations are shown in Figure 1.

3.1. Analysis of CCD Data

[18] After vetting, the data for each thermograph were smoothed with a 31-d boxcar filter to reduce tidal-induced fluctuations and to facilitate comparison with monthly sampling of solar insolation parameters in a later section. The resulting values at each depth were found to be very similar among the four sites. These smoothed data were averaged among the sites to obtain an island-wide average temperature per depth. The resulting time series are shown in Figure 3. A prominent feature in the series is the El Nino event of 1997 when temperatures at 30 m increased by 3°C.

[19] The temporal smoothing mitigates the short-term, tidal-induced, internal-wave temperature variations but may also introduce a bias. As an example, the original temperature data for the four depths at the Wrigley Institute of Environmental Studies (WIES) site are shown in Figure 4 for a time interval corresponding to maximum stratification, i.e., during the late summer. We find an asymmetry in the internal wave temperature modulations such that warm, surface water is occasionally transported to depth (30 m) and back to the surface, but cold water at depth is not brought to the surface. The asymmetry of these internal waves implies that the average temperature measured at depth is higher than what would be in the absence of internal waves. Presently, we neglect this effect but discuss its ramifications in a later section.

[20] Figure 3 indicates a major annual cycle that includes the expected warming beginning in the spring and reaching a maximum temperature in late August to September with the time of maximum varying with depth. The amplitude of the seasonal variations also changes with depth, decreasing from shallow to deep. Note that the seasonal variation is not a simple sinusoid but exhibits a narrow peak during the late summer and a short-period warming [*Norris*, 2003] in the late winter or early spring first noted by *List and Koh* [1976] as an anomalous warming.

[21] We quantify the annual variation by averaging daily temperatures among the years, the results of which are displayed in Figure 5. We fit the thermal modulation to a sinusoid with annual period, and with a mean value, amplitude, and phase determined empirically. Although the anomalous warming does not fit this simple model, its effects are an order of magnitude smaller than the major seasonal heating and therefore second order to the effects that we consider. The parameters obtained from the fit are listed in Table 4 along with the root-mean-square (RMS) of the model-data differences and uncertainty in the fitting parameters. The amplitude of the annual modulation is 3°C

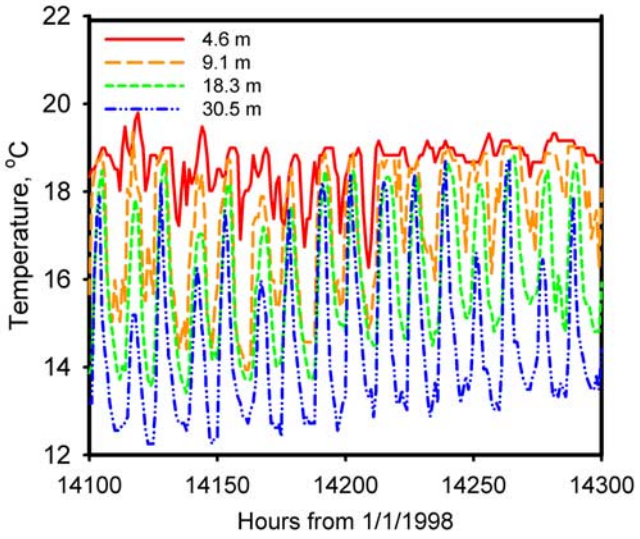

Figure 4. Example of WIES original temperature record for 200 h.

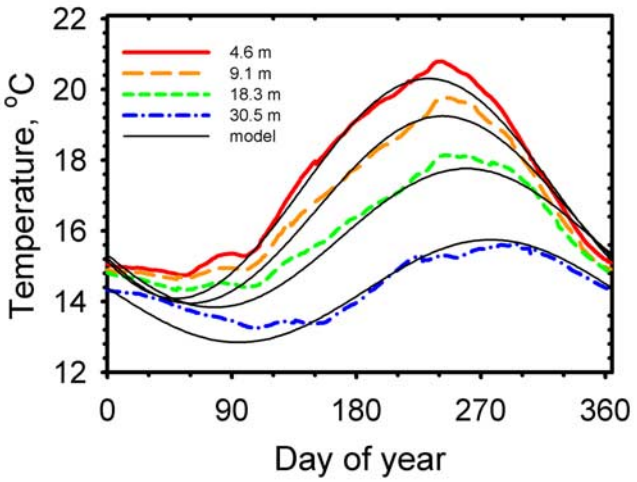

Figure 5. Average temperature for each depth at Santa Catalina and diffusion model with $\beta = 0.42$ m^{-1} and $\kappa = 0.00011$ m^2 s^{-1}.

near the surface and decreases to 1°C at 30.5 m. The day-of-year for temperature maximum is 230 for the near-surface data. At the 30.5-m depth it lags the near-surface phase by 53 days. The interdepth phase lag is unambiguous, as it is much larger than the phase-fitting error that is typically a couple of days. The RMS differences average 13% of the modulation amplitude.

3.2. Analysis of CalCOFI Data

[22] CalCOFI data were parsed into station, depth, and day-of-year and fitted to a sinusoid. The data were not sampled at the seasonal Nyquist; however, because the cruises were executed somewhat randomly over the years, when examined as a function of day-of-year, there is an apparent sampling that is greater than the seasonal Nyquist frequency for conditions of ergodicity. Values at a particular station and depth may be temporally separated by years so the interpretation of the fitted parameters is strongly dependent on the conditions of annual stationarity.

[23] Examples of the measured temperatures and retrieved parameters are shown in Figure 6 and listed in Table 5 for station 90.33, which is between Santa Catalina Island and the mainland. There were 94 measurements at this station over the 54 years under consideration. The surface data are nearly sinusoidal and the fit yields an amplitude of 2.86°C with maximum temperature occurring at day 243. The amplitude and temperature monotonically decrease with depth. The phase increases with depth progressing from day 243 at 0 m to day 358 at 50 m, with uncertainties of 3 and 10 d, respectively. That is, the warmest time of year for the surface water is in late August/September but it is in mid-December for the 50-m depth. The larger uncertainties in the fitted values for the CalCOFI data relative to those obtained with the CCD data are reflective of fewer CalCOFI samples.

[24] The CalCOFI temperature measurements were reduced to three-dimensional maps of the fitted parameters and displayed using Ocean Data View techniques (http://www.awi-bremerhaven.de/GEO/ODV). The temperature mean, amplitude and phase at 0, 10, 30, and 50 m are plotted as contour maps in Figure 7 through 9. For the deeper depths, the mean-temperature contours are parallel to the coastline. However, the shallow depths, 0 and 10 m, have a warm-water northeastern branch that intrudes into the center of the SCB. The amplitudes retrieved from the surface temperatures are large (2.5°C) in the center of the Bight and are easily distinguished from the rest of the CalCOFI data. At 10 m, this signal is still apparent, but disappears for the deeper depths.

[25] At the surface the phase is least (~day 240) for the center of the Bight and the continental shelf off Point Conception (34.5°N, 120.5°W) as compared to the phase further offshore into the CCS. The 10-m-depth phase indicates a delay in maximum temperature for the inner Bight but not for the CCS and the region off Pt. Conception. At 30-m depth, the maximum is later in the center of the Bight, but approximately the same offshore of Pt. Conception. The phase values at 50 m in some locations are providing high spatial frequency to the plot due to aliasing, but again, the phase at 50 m is similar throughout the CCS.

[26] To illustrate the phase behavior in the center of the Bight, a linear fit was performed on the phase versus depth data at each station from the surface to 30 m and plotted in Figure 10. The phase gradient has a maximum of 3 d/m in the center of the Bight. In contrast, the phase slope far offshore of the Bight is less than 0.5 d/m.

[27] We examined the CalCOFI salinity measurements in a similar manner as the temperature. The surface mean value and its uncertainty, in psu, are shown in Figure 11 as well as the amplitude and phase uncertainty. The spatial distribution of mean values is as expected: more saline values near the coast and fresher water found offshore. The seasonal amplitudes are disorganized and not large, typically 0.1 psu and the phase uncertainties are typically 100 d. There is no reliable seasonal salinity signal.

3.3. Analysis of NOAA Buoy Data

[28] Temperature measurements from each buoy were averaged to yield a value for each hour of the year and then smoothed over 745 h (31 d) with a boxcar filter and decimated 24:1 (daily sampling). The smoothed data are plotted in Figure 12 and the sinusoid fit parameters are listed in Table 6.

[29] All the buoy data exhibit a seasonal warming; however, there are noticeable variations among the sites. The largest mean temperature, amplitude and earliest maximum, are found at the Santa Monica buoy (46025).

[30] Three buoys outside of the Bight (46062, 46028, and 46042) indicate a southerly gradient with absolute temperatures increasing toward the south and that the amplitude of the seasonal variation decreases with increasing latitude.

Table 4. Mean, Amplitude, and Phase Fits for CCD Data

Depth, m	Mean Temp., °C	Amplitude, °C	Phase, Day of Year	RMS Diff., °C
4.6	17.2 ± 0.05	2.95 ± 0.07	230.3 ± 1.5	0.29
9.1	16.6 ± 0.00	2.46 ± 0.07	237.3 ± 1.7	0.34
18.3	15.8 ± 0.05	1.86 ± 0.07	249.7 ± 2.3	0.25
30.5	14.3 ± 0.05	1.09 ± 0.07	283.6 ± 3.9	0.16

The two buoys in or closest to the inner Bight (46025 and 46053) have the largest seasonal amplitude and mean temperature. They also peak in temperature earlier in the year, a month to a month-and-a-half earlier than the data for the other buoys. The Santa Monica buoy (46025) data fit is the best, having a RMS difference of nearly half that obtained with data from the other buoys.

[31] Note that both the Santa Barbara West buoy (46063) and the Tanner Banks buoy (46047) temperature data exhibit seasonal warming similar to many of the Central Coast stations. Both buoys are on the outer border of the SCB. However, the late winter-early spring cooling trend produced by the seasonal coastal upwelling is not present in the Tanner Banks data, which is situated furthest from the coast.

[32] The NOAA buoys also provide surface wind-velocity data. We have plotted a smoothed (31-d boxcar smoothing, daily sampling) speed (Figure 13) and direction (Figure 14) for two buoys within the Bight (46025 and 46053) and two bordering the Bight (46047 and 46062) with the latter being representative of the other three Central Coast buoys. The smallest wind speed is found in the inner Bight at 3 m/s during the early summer. In the northern Bight the speed is usually higher by 1 m/s but is seasonally more complex. Speeds at the other two buoys bordering the Bight are much larger, averaging about 6–7 m/s throughout the year and with higher variability. The wind direction for the outer buoys is relatively constant at 290°T most of the year, swinging between 290°T and 220°T during the winter months. In contrast, the wind direction in the inner Bight is 230°T most of the year.

3.4. Analysis of Other Long Time Series

3.4.1. Channel Islands National Park Data

[33] The retrieved parameters for all the ChINP sites are listed in Table 7. The uncertainty in the amplitude was generally 0.07°C while that of the mean was less than 0.1°C. There were little data from San Clemente, only 1 year in duration and the RMS difference was the largest there.

[34] The Northern Channel Islands (west to east: San Miguel, Santa Rosa, Santa Cruz, and Anacapa) approximate a one-dimensional chain along latitude 34°N. The analysis is simplified when the fitted parameters for the ChINP data are plotted as a function of depth and longitude in Figure 15. The data show that the mean and amplitude decrease, and the phase increases with increasing west-longitude and depth. Representative results for the amplitude, mean, and phase gradients with depth are 0.05°C/m, 0.025°C/m, and 1 d/m, respectively.

[35] The variation in longitudinal locations and depths among the sites obscures any north/south difference. However, for the site pair of Fry's Harbor and Gull Island off Santa Cruz (Figure 2), which are at the same longitude and nearly the same depth, the northern site (Fry's Harbor) leads in phase and has the greater seasonal amplitude. The values found for Fry's Harbor are the same as those found at the

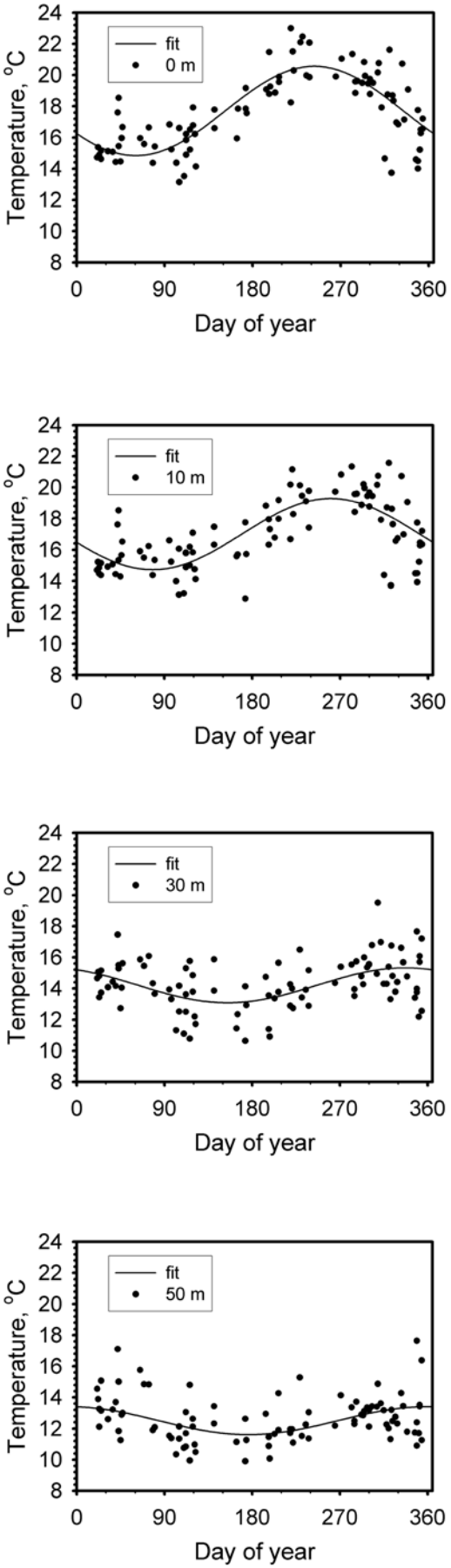

Figure 6. CalCOFI temperature measurements for 90.33 and fits.

Table 5. Mean, Amplitude, and Phase Fits for CalCOFI Data Line 90, Station 33

Depth, m	Mean Temp., °C	Amplitude, °C	Phase, Day of Year	RMS Diff., °C
0	17.6 ± 0.1	2.86 ± 0.15	243.1 ± 2.9	1.43
10	17.0 ± 0.1	2.28 ± 0.15	260.0 ± 3.7	1.50
20	15.6 ± 0.1	1.45 ± 0.14	298.3 ± 6.2	1.47
30	14.2 ± 0.1	1.13 ± 0.14	336.1 ± 7.8	1.42
50	12.6 ± 0.1	0.89 ± 0.15	358.2 ± 9.7	1.46

surface buoy in the eastern Santa Barbara Channel (46053). There is no phase gradient with depth for the measurements north of the island chain.

3.4.2. Scripps Pier and Oceanside

[36] We computed two sets of parameters for the Scripps Pier data: the first corresponding to the earlier regime and the latter chosen to correspond to the CCD measurement interval. Additionally, we digitized a 5-year temperature trace commencing on 1 October 1966, published by *List and Koh* [1976], of low-pass filtered surface temperature data for Oceanside, California, 40 km north of Scripps Pier. This region has a simpler submarine topography that is typical of coastal California south of the northern and central Bight. Fitted parameters to both Scripps Pier data intervals and the *List and Koh* [1976] plot are listed in Table 8. The values obtained for the earlier Scripps data and the Oceanside data, which are a temporal subset of the Scripps interval, are equivalent to those within the fitting uncertainties. Comparisons between the two intervals at Scripps Pier indicate a larger mean temperature and smaller phase for the latter interval and the same amplitude.

3.5. Regime Shift

[37] Local manifestation of the PDO, referred to as a regime shift by *Bograd and Lynn* [2003], was described as ocean temperature abruptly increasing by as much as 1°C in CalCOFI data. A review by *Mantua and Hare* [2002] also indicates a shift in wind stress over the Pacific basin. The two Scripps data intervals listed in Table 8 indicate the temperature difference between the two regimes as 1°C. The seasonal amplitude is 3.2°C for both intervals while the phase advances from 223 d for the interval before 1976, to 218 for the latter decades, a change that is slightly greater than the combined uncertainties.

[38] We have made similar calculations for the CalCOFI station nearest Santa Catalina Island that has significant sampling both before and after 1976. Data for station 90.33 were divided into two subsets straddling the regime change. Seasonal parameters are shown as a function of depth in Figures 16 through 18. The later subset has a higher mean temperature at all depths, about 0.7°C, though the stratification (vertical temperature gradient) of 0.1°C/m is the

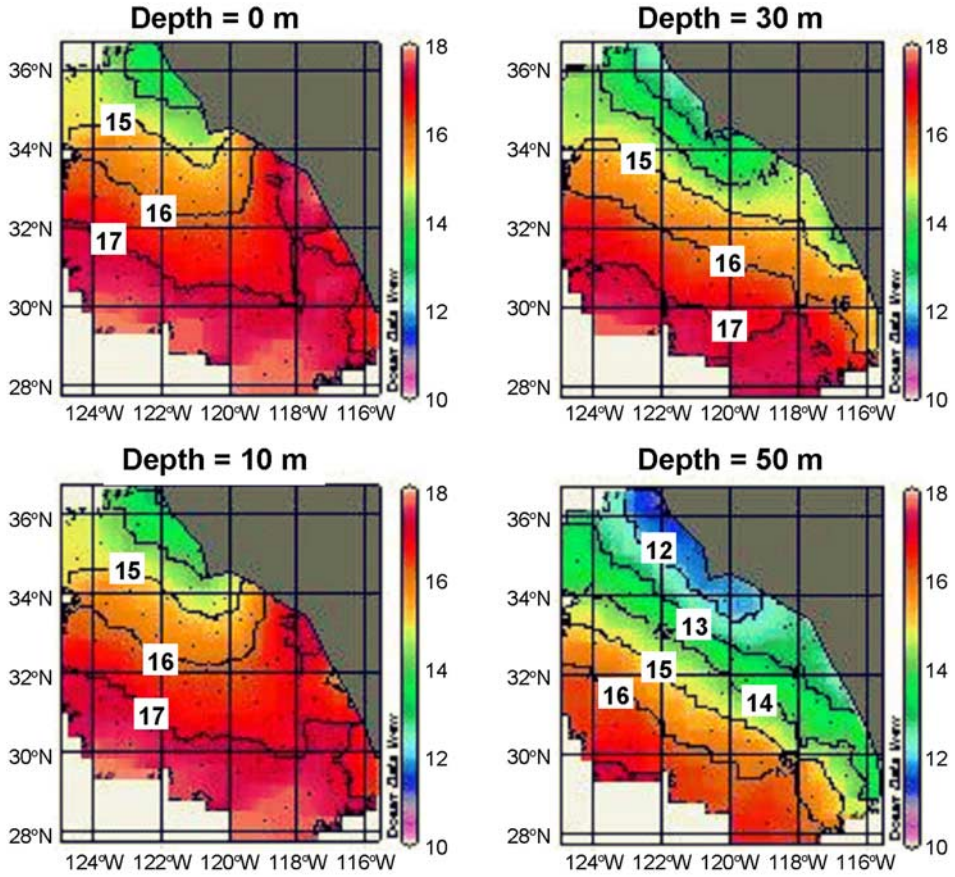

Figure 7. CalCOFI mean temperature at four depths.

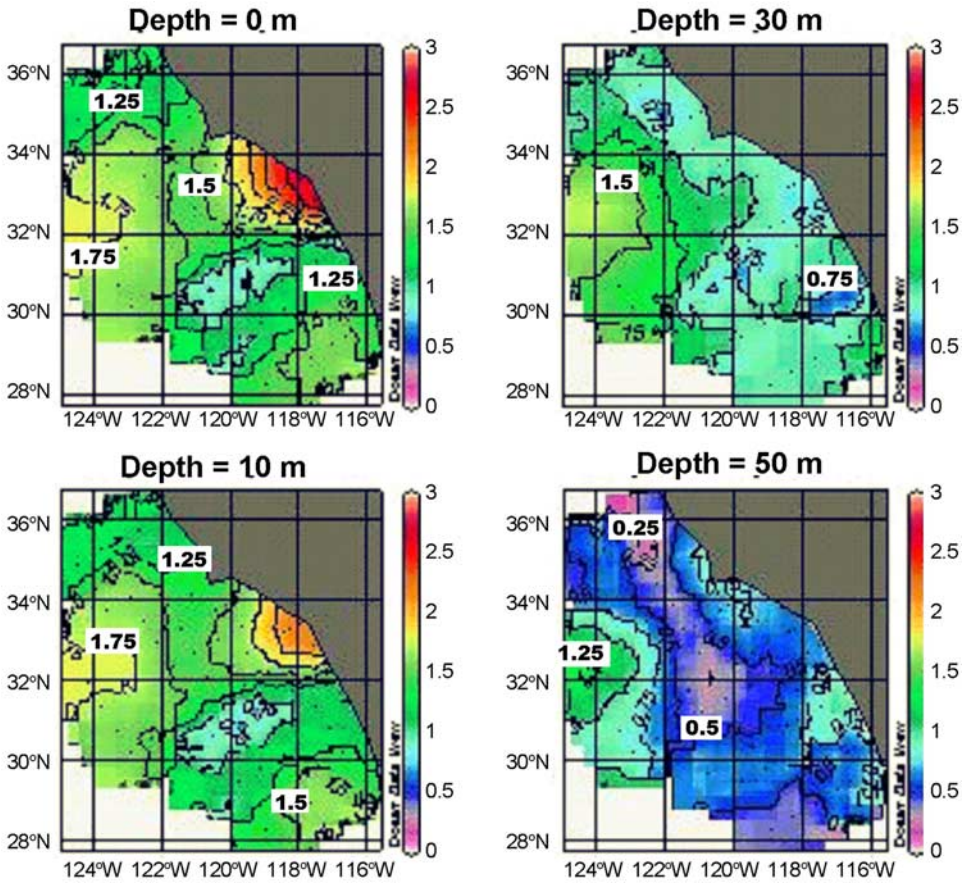

Figure 8. Amplitude of seasonal temperature variations from CalCOFI data.

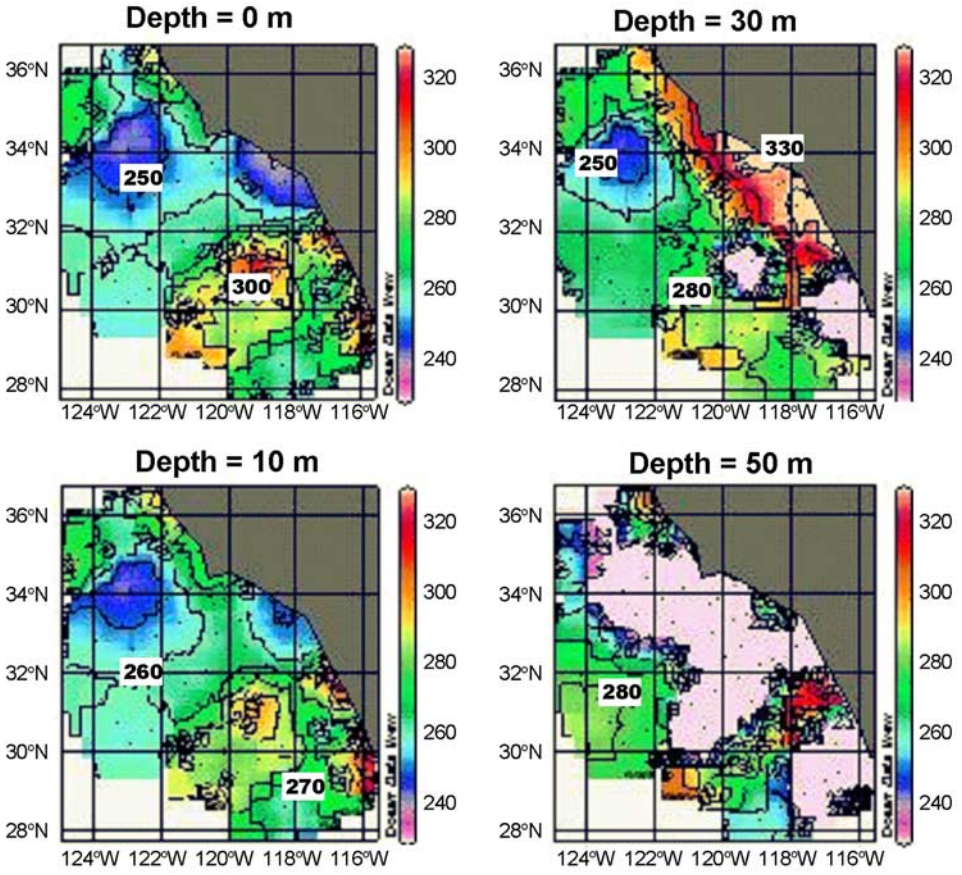

Figure 9. Day-of-year of maximum temperature for CalCOFI data.

same for both subsets. There are seasonal differences in the upper 10-m of the ocean, namely that the seasonal amplitude is greater by 1°C at the surface (Figure 17), and the maximum temperature occurs earlier in the later regime, Figure 18, by 30 d at the 10-m depth. Station 90.33 was well covered for both intervals, but in general, the stations are not so highly sampled to extend this study throughout the regions shown in the earlier CalCOFI figures without suffering large fitting uncertainties.

3.6. Comparisons Among Data Sets

[39] The data sets we analyzed were obtained from measurements executed with different techniques, at different locations and depths, and also made during different years. Comparison of data from adjacent CalCOFI stations and island sites generally agree. Differences between sites that are spatially separated are consistent with the spatial gradients measured with CalCOFI data.

[40] Our values for the fitted seasonal parameters of the CalCOFI data match those computed and made available by the CalCOFI organization. Their method differs from ours in that they execute a bi-harmonic fit and therefore fit for five parameters in contrast to our three. We also eliminated fewer station points from our calculations due to sampling considerations but retained the fitting uncertainty as a quality metric. We did eliminate stations that had very large uncertainty, such as those on line 97, which had very few samples for the first half of the calendar year. For specific

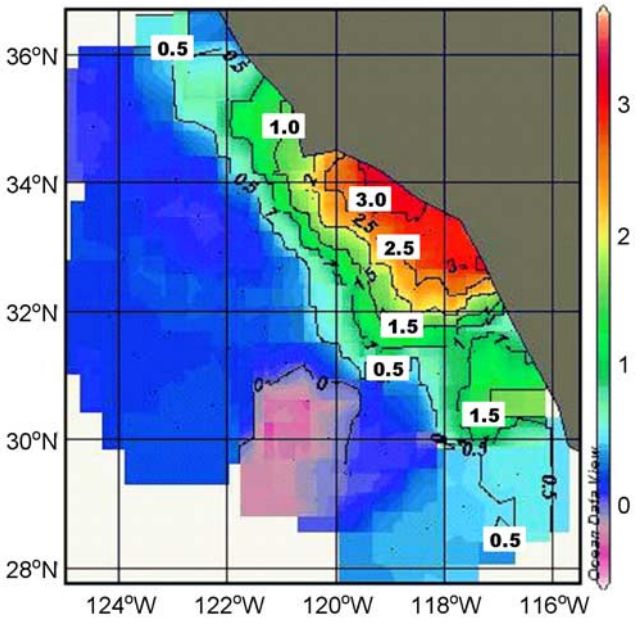

Figure 10. Phase vertical gradient, d/m, from CalCOFI data.

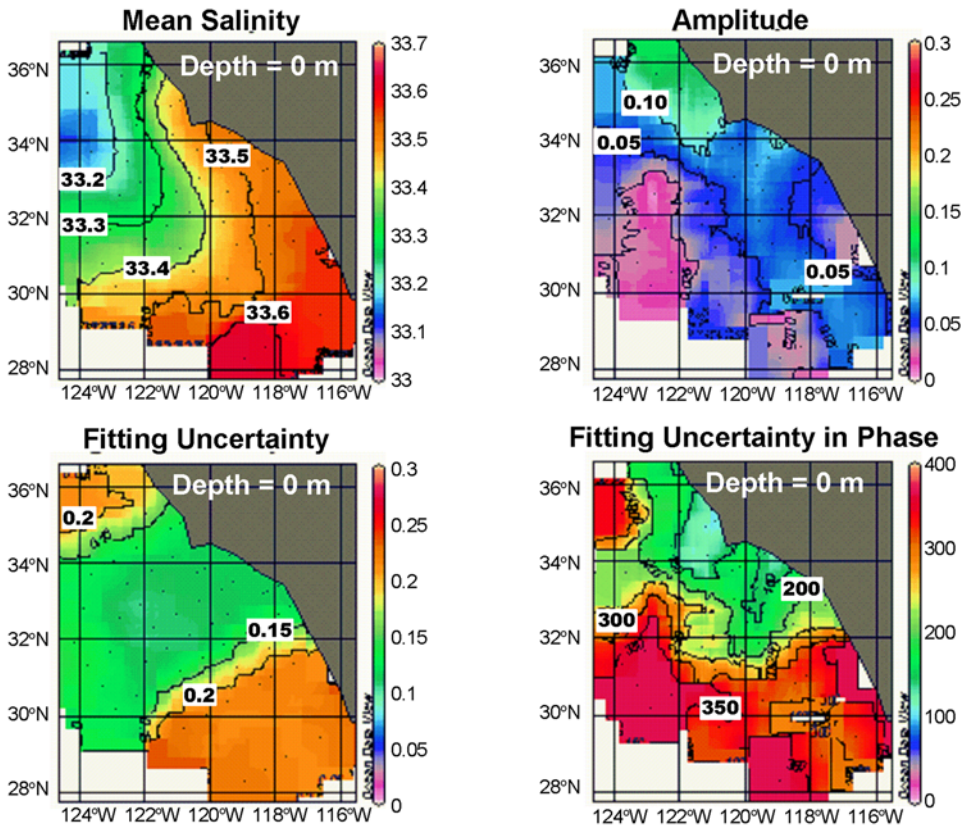

Figure 11. CalCOFI mean salinity (upper left) and fitting uncertainty (lower left). Salinity seasonal amplitude (upper right) and phase uncertainty (lower right) in days.

stations, we compared the amplitude and phase for CalCOFI-computed annual components to those obtained here and the differences are insignificant. We found that the semiannual components are unimportant and when included in our fitting process do not significantly change the annual components.

[41] There are only two data sets that give upper-ocean temperature and permit the calculation of the change in phase with depth: CalCOFI and CCD. When both data sets are used in their entirety the phase at Santa Catalina Island leads that determined by CalCOFI and the difference is larger for deeper depths (see Tables 4 and 5). The CalCOFI results depend strongly on the regime used. To eliminate this effect in the comparisons, we retrieved CalCOFI temperature data only for the years that the CCD array was operating. Using the nearest station to the island for these years, station 90.35, we compare mean temperatures, seasonal amplitudes and phases. When interpolated to the same depths, the CCD mean temperatures agree with the CalCOFI values. However, the phase at the CCD array is systematically smaller than that measured by CalCOFI, though the error bars overlap for the middle depths.

[42] The nature of the measurements, independent samples gathered over a decade, makes a systematic temporal measurement-bias unlikely. The CCD data were smoothed with a zero phase-shift filter that could not induce this phase change. We have identified two other possible sources of phase bias. First is the CalCOFI interpolation scheme, but when examined quantitatively, it does not account for the observed effect.

[43] The second source of bias is produced by the large internal waves found on the island's steep ($\sim 6^{\circ}$) slope. These waves exhibit rectification, i.e., warm surface water is brought to depth, but cold at-depth water is not transported

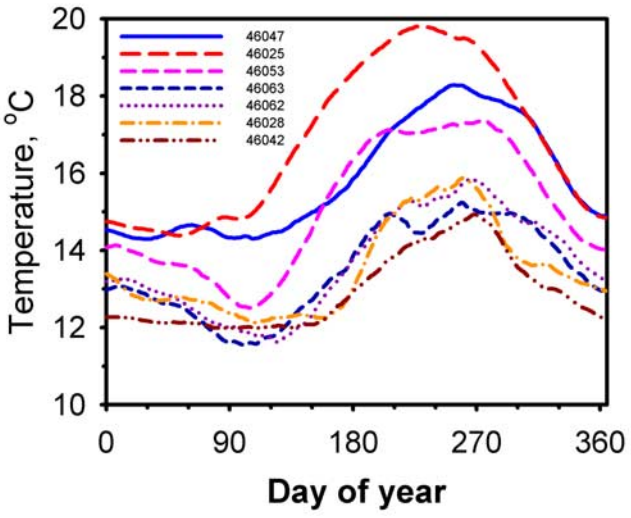

Figure 12. NOAA buoy temperature data.

Table 6. Mean, Amplitude, and Phase Fits for NOAA Buoys

ID	Depth, m	Mean Temp., °C	Amplitude, °C	Phase Day of Year	RMS Diff., °C
46047	0.6	15.9 ± 0.04	2.00 ± 0.05	257.0 ± 1.5	0.46
46025	0.6	16.9 ± 0.05	2.81 ± 0.07	229.3 ± 1.5	0.27
46053	0.6	15.1 ± 0.04	2.27 ± 0.05	250.0 ± 1.3	0.53
46063	0.6	13.5 ± 0.04	1.64 ± 0.05	264.0 ± 1.4	0.45
46062	0.6	13.7 ± 0.04	1.81 ± 0.05	269.4 ± 1.7	0.44
46028	0.6	13.5 ± 0.04	1.48 ± 0.05	260.7 ± 2.1	0.67
46042	0.6	12.9 ± 0.04	1.28 ± 0.05	257.2 ± 2.4	0.43

to the surface. The effect is also more pronounced for the deeper depths because the amplitude of the internal waves is greater there as measured by the temperature change (Figure 4). We quantitatively evaluated this effect using an empirical model for the internal waves and estimates of their amplitudes from temperature power spectral density measurements published in the work of *Gelpi and Norris* [2005]. At the deeper CCD-site depths this effect will reduce the phase and increase the mean and amplitude. It can account for 10 d of phase bias at 30 m, and 0.3°C in seasonal amplitude but will also decrease the mean temperature by 0.3°C. The first two effects are consistent with the CCD-CalCOFI data differences. However, the mean temperature for the CCD array is less than the CalCOFI measurements and compensation for the internal-wave bias will further separate them. CalCOFI station 90.35 is expected to have a higher mean temperature than the average of the CCD array as given by the spatial patterns in Figure 7, but not 0.5°C as determined by the internal-wave model.

[44] *Nezlin et al.* [2004] analyzed data from long-duration temperature monitoring by the Southern California Coastal Water Research Project (SCCWRP). They found the mean sea-surface temperature in the Santa Monica Bay to be 16.9°C and its seasonal amplitude to be 2.76°C with a phase of 229 d. These values agree with the Santa Monica buoy results and are very similar to those obtained at 4.6 m at Santa Catalina Island, 50 km to the south, but not with the CalCOFI data. They also measured salinity and report seasonal amplitude but not an uncertainty. Inspection of their scatter plots of salinity versus day-of-year suggests to us that the salinity phase is ambiguous, consistent with the results presented earlier in this paper.

[45] The work presented here is consistent with that of *Lynn* [1966]. He performed a biharmonic analysis of 13 years of CalCOFI temperature and salinity data for the 10-m depth. His plots also show that the inner Bight achieves maximum temperature earlier at the 10-m depth. His mean values agree well with those presented in Figure 7. His seasonal variations indicate the large amplitude in the inner Bight, consistent with Figure 8. The seasonal temperature maximum is largest in the inner Bight. He also finds a high-temperature tongue that reaches the San Diego area. He describes an isolated warm region off San Diego in terms of current flow and a bifurcation of water flowing into the Southern California Eddy. Finally, he notes the small seasonal salinity signal and that statistical tests indicate that nonseasonal variation dominates the salinity record.

[46] *Bograd and Lynn* [2003] have computed harmonic fits to the stratification, i.e., the temperature difference between the 10 and 150-m depths for the two regimes, 1950–1976 and 1977–1999, for four stations, including 90.37. They find that the maximum in stratification occurs earlier in the year for the latter interval. These differences are consistent with our observation that the phase of maximum temperature has moved to earlier in the year in the inner Bight. They note that during the latter years the recirculation eddy is weaker.

[47] With the minor exception of the Santa Catalina 30-m mean temperature, the various data sets are consistent among themselves and our results agree with those of other researchers when using the same data sets.

4. Seasonal Temperature Modulation and Model

[48] Observations of the seasonal temperature change in the top 30 m of water for the inner Bight indicate that relative to adjacent regions the seasonal amplitude is greater, the maximum temperature occurs earlier in the year, and the phase progresses with depth. In addition, there is no clear seasonal salinity signal. These dynamics suggest that local thermal conditions significantly affect the seasonal temperature properties rather than lateral advection of temperature gradients produced by different water sources. Here we compute the expected seasonal dynamics for this assumption using a simple model forced by the local solar insolation.

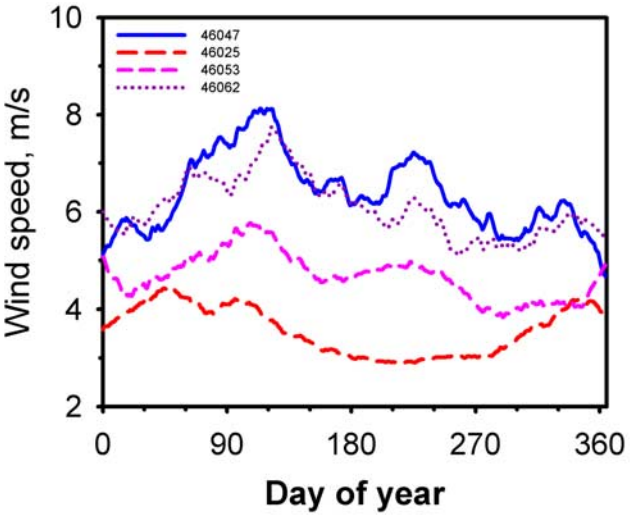

Figure 13. Average wind speeds for selected NOAA buoys.

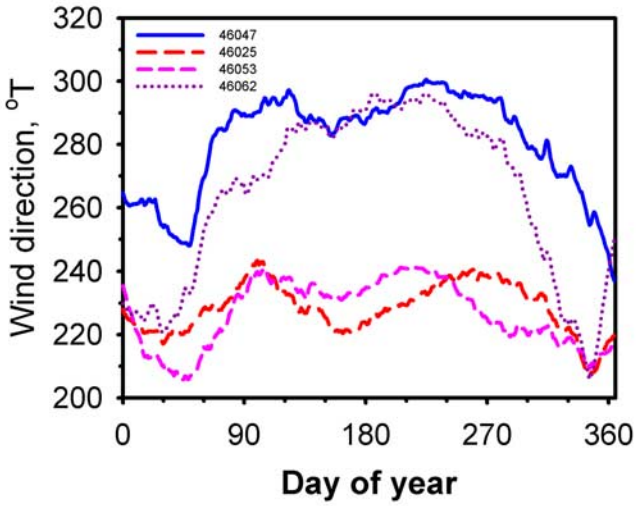

Figure 14. Average wind directions for selected NOAA buoys.

[49] We decompose the vertical solar flux into time-independent and time-dependent terms:

$$L(t) = L_0 + L_1 e^{-i\omega t}.$$

Here, L_0 and L_1 are the constant and seasonal energy flux in Wm^{-2}, respectively, and ω is the annual angular frequency. We model the divergence of the flux produced by absorption in the water column as an exponential. Using the heat equation described by *Gill* [1982] with the additional assumption of no advection the temperature must satisfy the forced diffusion equation:

$$\frac{\partial T}{\partial t} = \kappa \frac{\partial^2 T}{\partial z^2} + C e^{-\beta z} e^{-i\omega t}.$$

where

T the temperature in °C;
z the depth in m;
C the amplitude of the seasonal temperature modulation in °C/s;
ω the seasonal angular frequency in rad/s;
β the optical absorption depth in inverse meters;
κ the diffusion coefficient in $m^2 s^{-1}$.

[50] We decompose the temperature into time dependent and independent terms, too:

$$T(z,t) = T_0(z) + T_1(z,t)$$

[51] One boundary condition is that the seasonal temperature modulation, T_1, diminishes as the depth increases. If we assume that the diffusion and attenuation coefficients are depth-independent over the shallow range (30 m) of depths considered and the temperature modulation is sinusoidal, then the solution for T_1 satisfies

$$\frac{\partial^2 T_1}{\partial z^2} + \alpha^2 T_1 = -C' e^{-\beta z} e^{-i\omega t}, \tag{1}$$

with $\alpha^2 = i\omega/\kappa$ and

$$C' = \frac{L_1 \beta}{c_P \rho \kappa},$$

where ρ and c_p are the density and heat capacity of seawater, respectively. The solution is

$$T_1(z,t) = \frac{C'}{2i\alpha}\left[\frac{e^{-\beta z} - e^{i\alpha z}}{(i\alpha + \beta)} + \frac{e^{-\beta z}}{(i\alpha - \beta)}\right] e^{-i\omega t}. \tag{2}$$

Table 7. Fits to Seasonal Parameters for ChINP Data

Site	Island	Mean, °C	Amp., °C	Phase, d	RMS, °C	Depth, m
AR, Admiral's Reef	Anacapa	15.2 ± 0.05	2.0 ± 0.07	251.8 ± 2.1	0.40	16
CC, Cathedral Cove	Anacapa	15.9	2.6	240.0 ± 1.6	0.45	6
LC, Landing Cove	Anacapa	15.9	2.5	242.2 ± 1.7	0.44	5
AP, Arch Pt.	Santa Barbara	15.8	2.3	239.7 ± 1.9	0.43	8
CAT, Cat Canyon	Santa Barbara	16.0	2.2	239.8 ± 1.9	0.38	8
SESL, SE Sea Lion Rookery	Santa Barbara	14.5	1.8	254.5 ± 2.4	0.38	15
FH, Fry's Harbor	Santa Cruz	15.1	2.3	250.6 ± 1.9	0.51	13
GI, Gull Island	Santa Cruz	15.1	1.6	266.2 ± 2.6	0.39	15
PB, Pelican Bay	Santa Cruz	14.3	2.4	242.7 ± 1.8	0.54	8
SA, Scorpion Anchorage	Santa Cruz	15.2	2.5	244.8 ± 1.7	0.58	5
YB, Yellow Banks	Santa Cruz	15.5	1.9	252.3 ± 2.3	0.39	15
HR, Hare Rock	San Miguel	13.9	1.5	268.9 ± 2.8	0.39	5
WL, Wyckoff Ledge	San Miguel	12.5	1.3	298.9 ± 3.3	0.33	13
JLNO, Johnson's Lee North	Santa Rosa	15.5	1.8	259.2 ± 2.4	0.49	11
JLSO, Johnson's Lee South	Santa Rosa	14.2	1.2	276.8 ± 3.5	0.38	16
RR, Rodes Reef	Santa Rosa	13.5	1.6	261.1 ± 2.7	0.39	13
BSC, Boy Scout Camp	San Clemente	16.1	1.8	240.5 ± 2.4	0.84	11
EP, Eel point	San Clemente	15.8	1.4	248.5 ± 3.1	0.72	10
Horse Beach Cove, HBC	San Clemente	15.7	1.3	251.6 ± 3.3	0.74	13
NWH, North West Harbor	San Clemente	15.9	1.6	257.3 ± 2.8	0.85	11

For near-surface energy deposition the time-independent component must satisfy

$$\frac{\partial T_0}{\partial z} = \frac{-L_0}{c_p \rho \kappa}, \tag{3}$$

that is, the temperature depth-gradient is constant. Equation (3) provides an independent computation for κ.

4.1. Model Input and Output

[52] We computed the seasonal variation in surface fluxes at Santa Catalina Island from results retrieved from the NCEP/NCAR Reanalysis Project [*Kalnay et al.*, 1996]. The long-term monthly averages for the short-wave, long-wave, sensible-heat, and latent-heat energy fluxes were obtained from the web site, and assigned to the middle of the month. The constituent fluxes, the net flux, and a sinusoidal fit to the net flux are shown in Figure 19 and the fitted parameters listed in Table 9. We note that both *Winant and Dorman* [1997] and *Bograd et al.* [2001] determine flux values for the Bight from an analysis of in situ data (NOAA buoys and CalCOFI results). The net energy flux from *Bograd et al.* [2001] (86 Wm^{-2}) agrees with the reanalysis project results, but that from *Winant and Dorman* [1997] is almost a factor of 2 larger with a smaller seasonal amplitude. As the latter values are not reported for the seasonal Nyquist, we only used the reanalysis results.

[53] We estimated β and κ with a chi-squared minimization technique for the differences between the model of equation (2) and the Santa Catalina Island temperature data, obtaining $\beta = 0.425 \pm 0.025$ m^{-1} and $\kappa = 1.1 \pm 0.02 \times 10^{-4}$ m^2 s^{-1}. Model results with the addition of the temperature means are compared to the measurements in Figure 5. The overall amplitude, phasing, and depth dependence of these parameters match the data well.

[54] The same diffusion mechanism must transport downward the non-varying component of the input radiation, i.e., 83 W/m^2 via equation (3). Using a temperature gradient of 0.13°C m^{-1} (obtained from either CalCOFI or internal-wave adjustment of the CCD data), the resulting value for κ is 1.6×10^{-4} $m^2 s^{-1}$. This value is slightly larger than that determined from the seasonal forcing used above. Differences between the values of the diffusion coefficient measured using the seasonal forcing and the steady-state method may indicate the role of lateral advection or horizontal conductivity.

5. Summary and Discussion

[55] We have analyzed several long-duration temperature data sets for the SCB and surrounding region, including data from the Northern Channel Islands, Santa Catalina Island, CalCOFI cruises, NOAA buoys, and Southern California pier sites. Our data reduction consists primarily of retrieving values for the mean, amplitude, and phase of the annual temperature and salinity cycle. The amplitude is largest in the inner SCB and decreases with increasing distance from shore. The phase at the surface increases with distance such

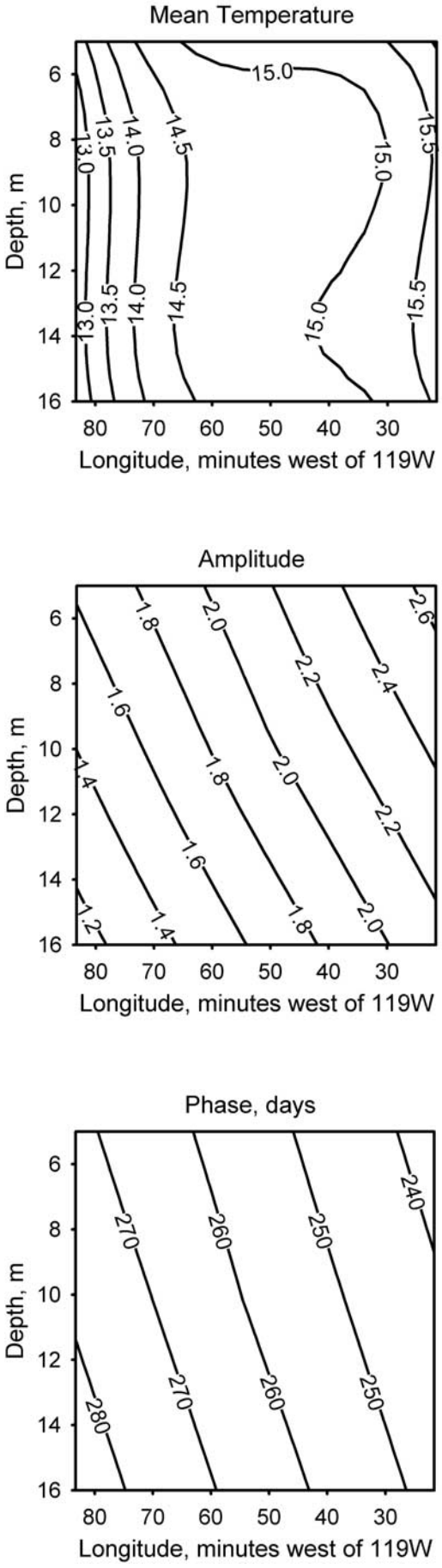

Figure 15. Fitted parameters for ChINP data: (a) mean temperature, (b) seasonal amplitude, and (c) seasonal phase, d.

Table 8. Mean, Amplitude, and Phase Measurements of Pier Data

Site	Depth, m	Mean Temp., °C	Amplitude, °C	Phase Day of Year	RMS Diff., °C
Scripps Pier 1956–1976	surface	16.8 ± 0.05	3.16 ± 0.07	223.6 ± 1.4	0.39
Oceanside 1966–1971	surface	16.8 ± 0.11	3.20 ± 0.16	223.0 ± 2.9	0.85
Scripps Pier 1992–2002	surface	17.8 ± 0.05	3.19 ± 0.07	218.4 ± 1.4	0.43

that the inner Bight peaks first in temperature. Within the inner Bight, there is a phase progression with depth such that the maximum temperature on the surface occurs about 6 weeks earlier than the maximum at 30 m. This effect also decreases with distance from shore such that in the California Current, the same phase (275 d) is found throughout the upper water column. The Northern Channel Islands apparently form a northern boundary regarding the phase gradient as it is not apparent in limited seasonal depth coverage north of the island chain but is found south of it. We find no significant seasonal salinity signal. *Palacios et al.* [2004], analyzing eight areas in the CCS, note that the SCB displays the largest *dT/dz* with mostly stationary seasonal cycles, consistent with our results.

[56] These observations suggest that local processes control the thermodynamics within the inner Bight. The large seasonal temperature variation and smallest phase there, together with the horizontal mean temperature gradient, indicates that lateral advection of the mean-temperature gradients alone cannot produce the inner Bight dynamics. Because the deeper depths are warming when the upper layers are cooling, the effect is not due to upwelling. Finally, the fact that there is no salinity signal although there is a mean-salinity horizontal gradient is consistent with the dynamics being produced by local sources and not lateral advection. We note that *Di Lorenzo et al.* [2005], in an analysis of 50 years of CalCOFI data, found that changes in oceanic advection are not the dominant mechanism for upper-ocean temperature changes. They state that the temperature changes must be produced by surface forcing functions.

[57] With no advective terms, the one-dimensional diffusion equation applies. *Jassby and Powell* [1975] used this equation to compute diffusion parameters numerically from temperature measurements as a function of depth and time for a lake. We have computed analytically the response to the local, seasonal energy fluxes using the 1-D equation with a sinusoidal forcing term. The solution is dependent on the vertical eddy-diffusion coefficient and the absorption scale length of shortwave radiation, both assumed to be constant over the top 30 m. We fit the analytic solution to the CCD data and retrieve the diffusion and absorption coefficients, on the order of 10^{-4} m^2 s^{-1} and 0.4 m^{-1}, respectively. The quantitative solution is in good agreement with the observations at Santa Catalina Island, yielding the correct absolute phase and amplitude as a function of depth.

[58] This value for the absorption coefficient is consistent with other data for this location and similar coastal areas. *Nezlin et al.* [2004] have conducted long-term transmissivity measurements in the inner Bight. Although not measuring absorption directly, the extinction (i.e., the absorption plus scattering) corresponding to their transmissivity measurements is greater than, and therefore consistent with, the absorption suggested here. Similar results were obtained from transmissivity measurements reported by *Hickey* [1992]. In a detailed analysis of the heating rate and solar transmission in near-surface coastal waters off New Jersey, *Chang and Dickey* [2004] measure absorption coefficients that are similar to the 0.42 m^{-1} value used to construct the model in Figure 5.

[59] Past computations of the diffusion coefficient in the upper temperate ocean yielded disparate results. *Ledwell et al.* [2004] and *Oakey and Greenan* [2004] measured vertical diffusivity in the coastal zone with a coordinated experiment on the East Coast. Using dye dispersion, Ledwell et al. found a value for the vertical diffusion coefficient that is an order of magnitude smaller at the 70-m isobath than that derived here for the upper 30 m. Oakey and Greenan confirmed the smaller value using measurements of microturbulence.

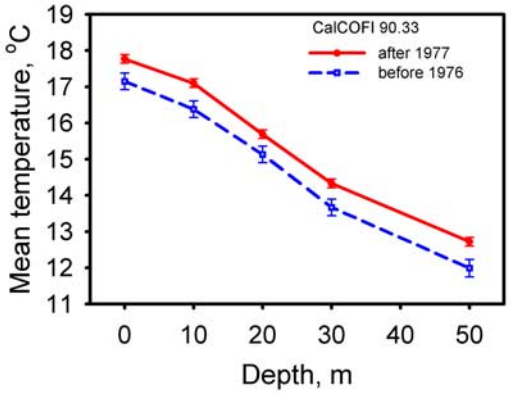

Figure 16. Seasonal means for the two regimes at station 90.33.

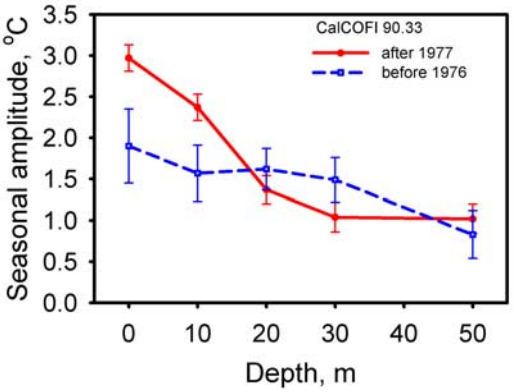

Figure 17. Seasonal amplitude for the two regimes.

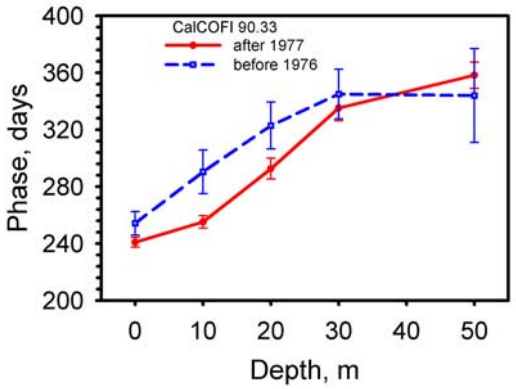

Figure 18. Seasonal phase for the two regimes.

[60] Vertical diffusion coefficients consistent with our values have been measured using computed nitrate transport for the near-surface euphotic zone. *King and Devol* [1979] computed values ranging from 0.05×10^{-4} m^2 s^{-1} to 1.1×10^{-4} m^2 s^{-1} off the west coast of Central America. *Eppley et al.* [1979], using similar techniques, reported values of $0.8–4.0 \times 10^{-4}$m^{2}s^{-1} in the near-surface waters of the SCB, including stations along CalCOFI line 90 near Santa Catalina Island. However, we note that all the above results were obtained from a handful of cruises and stations which are subject to episodic events. The influence of episodic events is lessened in the long-term time series used in the present work.

[61] The 1-D equation indicates that the mean temperature gradient with depth should be linear. Linear gradients of 0.11° m^{-1} and 0.13°C m^{-1} are found in the CCD and CalCOFI data, respectively. Indeed, the diffusion coefficients computed from the mean and seasonal variations (1.1×10^{-4}m^{2}s^{-1} and 1.6×10^{-4} m^2 s^{-1}, respectively) are closer than the range of estimates produced by other techniques, as shown above. However, the diffusion coefficient derived from the seasonal modulation does not support the transport of all net surface energy flux to deeper depths. This energy difference suggests that there is lateral advection with heat transported out of the inner Bight by currents on the order of 0.10 m/s. Such a large current appears to be inconsistent with the assumed small advection used to invoke the 1-D diffusion equation. However, a substantial eddy field can entrain water long enough to support vertical diffusion as the dominant mechanism while transporting excess heat away. Vestiges of such current systems have been found in the SCB. On a larger scale the Southern California Eddy, mentioned in section 2, appears as a closed loop when the dynamic height or its derived currents are averaged. In synoptic plots a closed loop is rarely found, implying an eddy field. Also there is an active smaller eddy field in the inner Bight as seen in synthetic aperture radar (SAR) images [*DiGiacomo and Holt*, 2001], radar measurements of currents [*Beckenbach and Washburn*, 2004] and satellite SST [*Hickey*, 1992]. Ocean advection is the inferred mechanism for seasonal heat budget closure outside of the Bight in the California Current. *Edwards and Kelly* [2007] compute differences between the energy input and the heat storage rate and attribute the phase difference to varying current flow.

[62] The CalCOFI retrieved parameters differed between regimes of the PDO. Both the amplitude and the phase were smaller during the cold phase (pre-1977). The Scripps Pier data also indicate that the phase has decreased from earlier times, though not the amplitude. We have not repeated our 1-D solution of the diffusion equation for the temperature values found in the pre-1977 regime because of the sparse sampling.

[63] The 1-D solution deviates most from the observed temperatures during the winter months. As discussed in section 2 this is the time of strong poleward flow of the countercurrent. This poleward flow may violate the no advection assumption, transporting warm water through the inner Bight so as to maintain a higher temperature than what the local radiative model suggests.

[64] The success of the simple diffusion equation in accounting for both the absolute amplitude and phase of the seasonal temperature modulation suggests that the assumption has merit. If so, there are interesting implications and derived problems.

[65] First, the upper-ocean thermodynamics in the inner Bight are not produced by the lateral advection of temperature gradients. The surface water must remain in the inner Bight long enough to undergo the annual cycle, about 9 months, or as long as there is a traceable temperature signal.

[66] Second, an effective vertical-diffusion coefficient for the upper 30 m of the surface can be computed. Although the diffusion coefficient is expected to be both depth and season dependent, a constant value appears to fit the data well. The vertical temperature gradient does not vary significantly with depth. To the extent that the diffusion coefficient is driven by the surface wind, we note that the wind speed in the Bight is fairly consistent throughout the year, see Figure 13, at about 3 m/s. It is larger in the winter when the temperature gradient diminishes.

[67] Third, the amplitude and phase for the cool period of the PDO suggest that the diffusion coefficient was larger then. However, assuming the same solar flux, non-varying vertical energy transport is the same for both the cool and warm periods (same *dT/dz,* Figure 16). The differences suggest that the upper-layer horizontal-transport in the Bight changed with the PDO cycle.

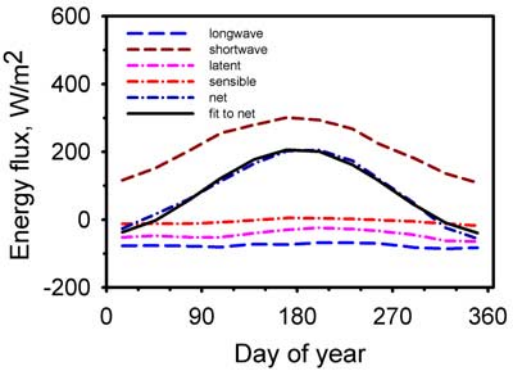

Figure 19. Surface fluxes at Santa Catalina Island from NCEP/NCAR Reanalysis project.

Table 9. Mean, Amplitude, and Phase Measurements for NCEP/NCAR Net Surface Flux

Mean Flux, W/m^2	Amplitude, W/m^2	Phase Day of Year	RMS Difference, W/m^2
82.7± 0.2	125.3± 0.3	180.7 ± 0.1	10.7

[68] Fourth, the diffusion mechanism suggests an explanation for the anomalous warming found in the CCD data during March. The warming is really driven by the phase of the seasonal flux as shown in Figure 5. However, it is interrupted by the onset of upwelling during the spring transition. In the analysis of cruise data gathered during a single spring transition, *Lynn et al.* [2003] measured temperature changes produced by the upwelling. Their results for the northern tip of Santa Catalina Island are the same as those measured simultaneously by the CCD array, indicating that for one event, the apparently anomalous warming is actually the early phase of the seasonal warming that precedes the spring upwelling.

[69] **Acknowledgments.** We thank all the CCD divers who contributed to the thermograph project, especially Ted Sharshan, John Turney, and Paul Meister, and WIES marine safety officer Derek Smith for his assistance with the local bathymetry measurements. We thank the National Park Service and David Kushner at the Channel Islands National Park for providing the ChINP data. We obtained the NOAA data from the National Data Buoy Center site www.ndbc.noaa.gov/archive.shtml. The NOAA-CIRES Climate Diagnostics Center, Boulder, Colorado, USA, provided the NCEP Reanalysis data through their Web site www.cdc.noaa.gov/cdc/data.ncep.reanalysis.derived.html#surface_gauss. CalCOFI data were provided through their Web site www.calcofi.org and Scripps data were obtained from http://shorestation.ucsd.edu/active/index_active.html#lajollastation. Mapping software was obtained from Ocean Data View (http://www.awi-bremerhaven.de/GEO/ODV).

References

Beckenbach, E., and L. Washburn (2004), Low-frequency waves in the Santa Barbara Channel observed by high-frequency radar, *J. Geophys. Res.*, *109*, C02010, doi:10.1029/2003JC001999.

Bograd, S. J., and R. J. Lynn (2003), Long-term variability in the southern California current system, *Deep Sea Res. II*, *50*, 2355–2370.

Bograd, S. J., T. K. Chereskin, and D. Roemmich (2001), Transport of mass, heat, salt, and nutrients in the southern California Current System: Annual cycle and interannual variability, *J. Geophys. Res.*, *106*(C5), 9255–9275.

Bratkovich, A. (1985), Aspects of the tidal variability observed on the Southern California shelf, *J. Phys. Oceanogr.*, *15*, 225–239.

Bray, N. A., A. Keyes, and W. M. L. Morawitz (1999), The California current system in the Southern California Bight and the Santa Barbara Channel, *J. Geophys. Res.*, *104*(C4), 7695–7714.

Chang, G. C., and T. D. Dickey (2004), Coastal ocean optical influences on solar transmission and radiant heating rate, *J. Geophys. Res.*, *109*, C01020, doi:10.1029/2003JC001821.

Chelton, D. B. (1982), Large-scale response of the California current to forcing by the wind stress curl, *CalCOFI Rep. XXIII*, Scripps Inst. of Oceanogr., Univ. of Calif., San Diego, La Jolla, Calif.

Cross, J. N., and L. G. Allen (1993), Fishes, in *Ecology of the Southern California Bight*, pp. 457–540, edited by M. D. Dailey et al., Univ. of Calif. Press, Berkeley, Calif.

Davis, G. E., D. J. Kushner, J. M. Mondragon, J. E. Mondragon, D. Lerma, and D. V. Richards (1997), *Kelp Forest Monitoring Handbook*, vol. 1, *Sampling Protocol*, Natl. Park Service, Washington, D. C.

DiGiacomo, P. M., and B. Holt (2001), Satellite observations of small coastal ocean eddies in the Southern California Bight, *J. Geophys. Res.*, *106*(C10), 22,521–22,543, doi:10.1029/2000JC000728.

Di Lorenzo, E., A. J. Miller, N. Schneider, and J. C. McWilliams (2005), The warming of the California current system: Dynamics and ecosystem implications, *J. Phys. Oceanogr.*, *35*, 336–362.

Earle, M. D. (1996), Nondirectional and directional wave data analysis and procedures, *NDBC Tech. Doc. 96-01*, Natl. Data Buoy Cent., Stennis Space Center, Miss.

Edwards, K. A., and K. A. Kelly (2007), A seasonal heat budget across the extent of the California current, *J. Phys. Oceanogr.*, *3*, 518530, doi:10.1175/JPO2990.1.

Eppley, R. W., E. H. Renger, and W. G. Harrison (1979), Nitrate and phytoplankton production in southern California coastal waters, *Limnol. Oceanogr.*, *24*(4), 645–651.

Gelpi, C. G., and K. E. Norris (2005), Seasonal and high-frequency ocean temperature dynamics at Santa Catalina Island, in *Proceedings of the Sixth California Islands Symposium, Ventura, California, December 1–3, 2003*, *Tech. Publ. CHIS-05-01*, edited by D. K. Garcelon and C. A. Schwemm, pp. 461–471, Natl. Park Service, Washington, D. C.

Gill, A. E. (1982), *Atmosphere-Ocean Dynamics*, Academic, San Diego, Calif.

Hamilton, P., M. A. Noble, J. Largier, L. K. Rosenfeld, and G. Robertson (2006), Cross-shelf subtidal variability in San Pedro Bay during summer, 2001, *Cont. Shelf Res.*, *26*, 681–702, doi:10.1016/j.csr.2006.01.009.

Hickey, B. M. (1992), Circulation over the Santa Monica-San Pedro Basin and Shelf, *Prog. Oceanogr.*, *30*, 37–115.

Hickey, B. (1993), Physical oceanography, in *Ecology of the Southern California Bight*, edited by M. D. Dailey et al., pp. 19–70, Univ. of Calif. Press, Berkeley, Calif.

Hickey, B. M., E. L. Dobbins, and S. E. Allen (2003), Local and remote forcing of currents and temperature in the central Southern California Bight, *J. Geophys. Res.*, *108*(C3), 3081, doi:10.1029/2000JC000313.

Jassby, A., and T. Powell (1975), Vertical patterns of eddy diffusion during stratification in Castle Lake, California, *Limnol. Oceanogr.*, *20*, 530–543.

Kalnay, E., et al. (1996), The NCEP/NCAR 40-year reanalysis project, *Bull. Am. Meteorol. Soc.*, *77*, 437–471.

King, D. F., and A. H. Devol (1979), Estimates of vertical eddy diffusion through the thermocline from phytoplankton nitrate uptake rates in the mixed layer of the eastern tropical Pacific, *Limnol. Oceanogr.*, *24*(4), 645–651.

Ledwell, J. R., T. F. Duda, M. A. Sundermeyer, and H. S. Seim (2004), Mixing in a coastal environment: 1. A view from dye dispersion, *J. Geophys. Res.*, *109*, C10013, doi:10.1029/2003JC002194.

Lerczak, J. A., C. D. Winant, and M. C. Hendershott (2003), Observations of the semidiurnal internal tide on the southern California slope and shelf, *J. Geophys. Res.*, *108*(C3), 3068, doi:10.1029/2001JC001128.

List, E. J., and R. C. Y. Koh (1976), Variations in coastal temperatures on the southern and central California coast, *J. Geophys. Res.*, *81*, 1971–1979.

Lynn, R. J. (1966), Seasonal variation of temperature and salinity at 10 meters in the California current, *CalCOFI Rep. XI*, Scripps Inst. of Oceanogr., Univ. of Calif., San Diego, La Jolla, Calif.

Lynn, R. J., and J. J. Simpson (1987), The California current system: The seasonal variability of its physical characteristics, *J. Geophys. Res.*, *92*(C12), 12,947–12,966.

Lynn, R. J., and J. J. Simpson (1990), The flow of the undercurrent over the continental borderland off southern California, *J. Geophys. Res.*, *95*(C8), 12,995–13,008.

Lynn, R. J., S. J. Bograd, T. K. Chereskin, and A. Huyer (2003), Seasonal renewal of the California current: The spring transition off California, *J. Geophys. Res.*, *108*(C8), 3279, doi:10.1029/2003JC001787.

Mantua, N. J., and S. R. Hare (2002), The Pacific Decadal Oscillation, *J. Oceanogr.*, *58*, 35–44.

Mendelssohn, R., F. B. Schwing, and S. J. Bograd (2004), Nonstationary seasonality of upper ocean temperature in the California current, *J. Geophys. Res.*, *109*, C10015, doi:10.1029/2004JC002330.

Neslin, N. P., J. J. Oram, P. M. DiGiacomo, and N. Gruber (2004), Subseasonal to interannual variations of sea surface temperature, salinity, oxygen anomaly, and transmissivity in Santa Monica Bay, California from 1987 to 1997, *Cont. Shelf Res.*, *24*, 1053–1082.

Norris, K. (2003), How to accurately predict water temperature at depth on your next Catalina dive, *Calif. Diving News*, *20*(2), 6–7.

Oakey, N. S., and B. J. W. Greenan (2004), Mixing in a coastal environment: 2. A view from microstructure measurements, *J. Geophys. Res.*, *109*, C10014, doi:10.1029/2003JC002193.

Palacios, D. M., S. J. Bograd, R. Mendelssohn, and F. B. Schwing (2004), Long-term and seasonal trends in stratification in the California current, 1950–1993, *J. Geophys. Res.*, *109*, C10016, doi:10.1029/2004JC002380.

Pidgeon, E. J., and C. D. Winant (2005), Diurnal variability in currents and temperature on the continental shelf between central and southern California, *J. Geophys. Res.*, *110*, C03024, doi:10.1029/2004JC002321.

Reid, J. L. (1988), Physical oceanography, 1947–1987, *CalCOFI Rep. XXIX*, Scripps Inst. of Oceanogr., Univ. of Calif., San Diego, La Jolla, Calif.

Winant, C. D., and A. W. Bratkovich (1981), Temperature and currents on the southern California shelf: A description of the variability, *J. Phys. Oceanogr.*, *11*, 71–85.

Winant, C. D., and C. E. Dorman (1997), Seasonal patterns of surface wind stress and heat flux over the Southern California Bight, *J. Geophys. Res.*, *102*(C3), 5641–5653.

C. G. Gelpi, Northrup Grumman XonTech Systems, 6862 Hayvenhurst Avenue, Van Nuys, CA 91406, USA. (craig.gelpi@ngc.com)

K. E. Norris, 15954 Leadwell Street, Van Nuys, CA 91406-3030, USA. (karen.norris@ngc.com)